Check for updates

Received: 2 April 2026 | Revised: 28 May 2026 | Accepted: 3 June 2026

DOI: 10.1002/aic.70513

AIChE JOURNAL

RESEARCH ARTICLE

Separations: Materials, Devices and Processes

Structured sorbents for Direct Air Capture: The impact of materials and chemicals on performance

Nicole Ferru[1] | Moritz Bischof[1] | Martina Saporito[1] | David Büchner[2] | Quirin Grossmann[1] | Vincent Dufour-Décieux[1] | Ronny Pini[2] | André Bardow[1] | Marco Mazzotti[1]

[1]Institute of Energy and Process Engineering, ETH Zurich, Zurich, Switzerland

[2]Department of Chemical Engineering, Imperial College London, London, UK

Correspondence
André Bardow and Marco Mazzotti, Institute of Energy and Process Engineering, ETH Zurich, 8092 Zurich, Switzerland.
Email: abardow@ethz.ch, marcom@ethz.ch

Funding information
ETH Zürich Foundation; Imperial College London

Abstract

Structured sorbents can efficiently process large air volumes required for Direct Air Capture (DAC), but their broad implementation is limited by challenges in producing reproducible and homogeneous materials. This work presents a robust procedure to graft amines onto monolithic sorbents and systematically investigates how CO_2 capture performance is influenced by three fundamental material building blocks: substrate type (mullite vs. cordierite), alumina loading, and amine type (APTMS vs. TRI). X-ray Computed Tomography and gravimetric analyses confirm uniform amine distribution, with CO_2 adsorption capacity scaling linearly with alumina mass. From a process perspective, lower density substrates achieve higher specific CO_2 uptake, thus reducing the energy demand for regeneration. Breakthrough experiments demonstrate that humidity significantly enhances adsorption thermodynamics and kinetics: CO_2 uptake increases by 30% for APTMS and 70% for TRI, and adsorption kinetics are accelerated. This study provides quantitative material performance relationships necessary for process design and contactor optimization.

KEYWORDS
adsorption, contactor optimization, Direct Air Capture, humidity, structured sorbents

1 | INTRODUCTION

Limiting global warming to well below 2°C above pre-industrial levels, as set out in the Paris Agreement,[1] motivates the rapid development and deployment of Direct Air Capture (DAC) technologies. While emission reductions are critical, DAC provides a necessary pathway to remove legacy CO_2 directly from the ambient air, addressing hard-to-abate sectors and achieving net-zero goals.[2–4] In particular, DAC can address emissions from distributed sources, which constitute 50% of current emissions.[5] When combined with permanent CO_2 storage, DAC offers a scalable route to net-negative emissions.[6]

For DAC, various technological approaches have been proposed, including liquid absorption, mineral looping, solid adsorption, and wet-electrochemical routes.[4] Among these strategies, solid sorbent systems stand out due to their potential for lower energy consumption. In particular, solid sorbents can be regenerated at comparatively mild temperatures, thereby reducing high-temperature thermal energy demand and facilitating integration with low-grade or renewable heat sources.[6]

Still, capturing CO_2 at ultra-dilute concentrations and ambient conditions poses challenges to material selection, contactor design, and process operation: The low concentration of CO_2 in ambient air

This is an open access article under the terms of the Creative Commons Attribution License, which permits use, distribution and reproduction in any medium, provided the original work is properly cited.
© 2026 The Author(s). *AIChE Journal* published by Wiley Periodicals LLC on behalf of American Institute of Chemical Engineers.

requires the sorbents to have a high affinity to CO_2. In addition, DAC technologies need to cope with various levels of humidity present in ambient air, which can strongly affect the separation efficiency and lifetime of the sorbent materials, and therefore process robustness.[6–8] The interactions between CO_2, humidity, and the sorbent are highly material-specific and complex, with some mechanisms having opposite effects on both adsorption equilibrium and mass transfer kinetics.[9,10] Physisorbents, such as zeolites and Metal-Organic Frameworks (MOFs), have been proposed for DAC applications. Physisorbents utilize high surface areas and tunable pore sizes to capture gas molecules selectively. Consequently, they offer high potential for long-term stability and lower regeneration energy.[11,12] However, many physisorbents face challenges such as poor selectivity, resulting in a low adsorption capacity in ultra-dilute conditions, particularly due to strong competition with moisture.[4] The most employed materials for DAC are therefore chemical sorbents.[13] Amine-functionalized sorbents, in particular, are among the most studied sorbents as they combine the high CO_2 affinity of amine groups leveraged in absorption, the low energy requirement for regeneration typical of adsorption, and an increased CO_2 adsorption capacity in the presence of humidity.[4,13–16] Amine-functionalized sorbents immobilize amines on porous solid supports by either impregnation or grafting, whereby the amines covalently bond to the hydroxy groups present on the surface of a metal-oxide.[13] For DAC, different amine structures have been considered, namely, (i) monoamines with only primary amine groups,[10,17] (ii) triamines featuring both primary and secondary amine groups,[10,14,17–19] and (iii) amine-containing polymers such as Poly(ethylenimine) (PEI).[20–23] While all amines increase uptake in humid conditions,[24] there is a trade-off between adsorption capacity and kinetics depending on the amine structure.[10,24] Most materials have been studied in the form of powders or beads[17,19,23,25–29] that are easy to produce and analyze.

Commercial applications of DAC plants, however, require efficient contactor geometries: The low CO_2 concentration in the atmosphere results in the need to process large volumes of air, which is associated with high energy requirements, making contactor designs with low resistance to airflow desirable.[12] For this reason, structured sorbents with low pressure drop have gained attention in recent studies and pilot applications.[14,30–36] Some studies have explored placing beads or pellets into structured frames.[32] A more direct and potentially more efficient solution are monolithic sorbents[14,35,37–42] or laminates,[30,34,43] where the structure and active material are intrinsically integrated. Despite their widespread use in catalysis and separations,[44] monoliths functionalized for DAC remain comparatively underexplored, in part due to challenges associated with achieving homogeneous and reproducible functionalization of such structures. Sakwa-Novak et al.[35] and Narayanan et al.[40] present self-supported PEI monoliths which achieve high CO_2 uptake and low energy penalty, as they do not have an inert substrate. However, the PEI adsorbents suffer from slow mass transfer kinetics associated with impregnated adsorbents. Grossmann et al.[14] propose a water-based grafting procedure for monoliths that minimizes mass transfer resistance[45] but suffers from high complexity. Kim et al.[39] developed a 3D printed contactor with tailored macro-geometries that achieves exceptional capture performance. While additive manufacturing techniques offer unprecedented control over transport phenomena,[39–41] the scalability challenges of 3D printed contactors remain significant hurdles for deployment. In contrast, industrially extruded ceramic honeycomb monoliths represent a mature and economically viable near-term solution.

In this work, we address these challenges by adapting a robust amine-grafting procedure to alumina-coated monolithic sorbents. We focus on monolithic sorbents consisting of an inert ceramic substrate, a microporous alumina coating, and covalently grafted amines. To provide a robust framework for material design and optimization, this work varies the three fundamental building blocks of the monolithic sorbents: the substrate type, alumina loadings, and amine types. The interactions between CO_2, humidity, and the resulting material are dependent on all three building blocks. Still, the functionalization procedure itself is designed to be applicable for all material variations, while ensuring a homogeneous distribution of the active phase throughout the monolith. The main goal of this work is to systematically decouple the influence of all three material features on the CO_2 capture performance under DAC conditions, including the effect of humidity. Ultimately, this investigation provides the foundational data necessary to utilize these structured sorbents for cycle design and optimization, and thus for the advancement of DAC technology.

2 | MATERIALS AND METHODS

2.1 | Materials

The sorbent material investigated in this work is a composite structure designed for CO_2 capture, composed of three main components, as schematically shown in Figure 1: an inert mesoporous ceramic substrate, a microporous $\gamma-$alumina coating, and grafted amines. Each of these components can be varied independently to study their influence on the overall capture performance. In particular, we test two substrate types (cordierite and mullite), a varying amount of alumina coating, and two amine types. The grafting procedure to immobilize the amines onto the alumina surface constitutes a key methodological development of this study, specifically designed and optimized to achieve reproducible and homogeneous functionalization of structured sorbents. A total of 25 samples are analyzed in this study. An overview of all the samples is provided in the Supporting Information S2.

2.1.1 | Substrate

Two types of monoliths are used in this study: Alumina-coated mullite monoliths were kindly provided by HUG Engineering (Switzerland). The monoliths are 130 mm long and have a squared cross section with edge length of 3 mm, a cell density of 100 CPSI (cells per square inch), a squared channel size of 2 mm × 2 mm and a wall thickness of

15475905, 2026, 10, Downloaded from https://aiche.onlinelibrary.wiley.com/doi/10.1002/aic.70513 by Imperial College London, Wiley Online Library on [15/09/2026]. See the Terms and Conditions (https://onlinelibrary.wiley.com/terms-and-conditions) on Wiley Online Library for rules of use; OA articles are governed by the applicable Creative Commons License

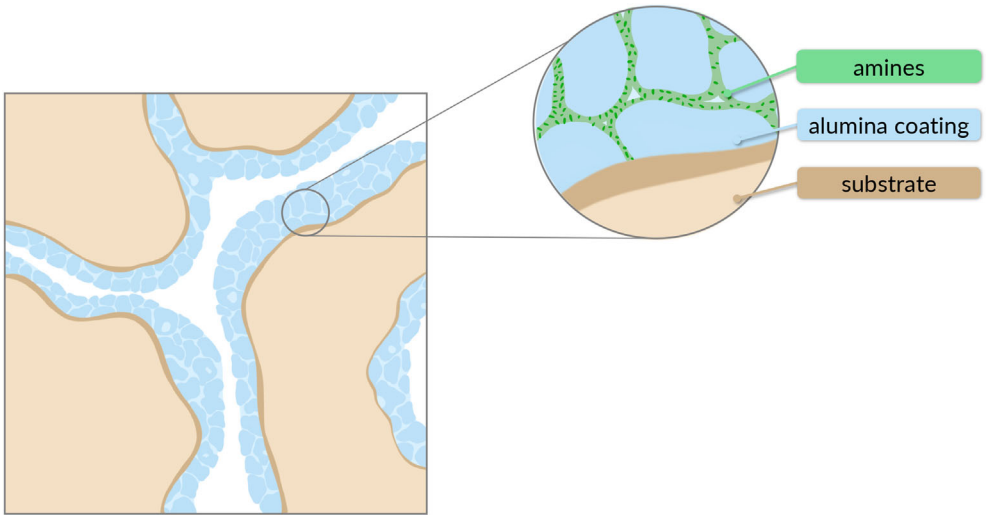


FIGURE 1 Schematic of the sorbent material considered in this work consisting of an inert, mesoporous ceramic substrate, a microporous $\gamma-$alumina coating and grafted amines. The magnified view shows the internal porous matrix of the γ-alumina coating, illustrating that the grafted amines reside within the inner pore channels.

0.4 mm. The ceramic substrate is first extruded and subsequently wash coated with γ-alumina. The wash coating was performed by the manufacturers by dipping the monoliths into a dispersion of Sasol Pural TH 200 in water, followed by calcination at 500°C for 1 hour.

The alumina-coated cordierite monoliths were kindly provided by Corning (USA). These monoliths have the same length and width, but a higher cell density of 200 CPSI, squared channel size of 1.5 mm × 1.5 mm, and a wall thickness of 0.2 mm. The cordierite monoliths are also extruded and subsequently wash coated by Corning by dipping the monoliths into a dispersion of Sasol Pural TH 200 in water, followed by calcination at 550°C for 3 hours.

For both monolith types, the coating amount is increased by increasing the concentration of Sasol Pural TH 200 solution and by repeating the dipping multiple times.

The resulting alumina loading α of both monolith types is defined as:

$$\alpha = \frac{m_{al}}{m_{sub}} \quad (1)$$

where m_{al} is the mass of alumina and m_{sub} is the mass of the ceramic substrate. The alumina loading ranges from 10 wt.% to 32 wt.% for the mullite monoliths, and 14 wt.% to 70 wt.% for the cordierite monoliths. The main difference between the two substrates is that the mullite walls have larger pores, lower porosity, and therefore higher bulk density than the cordierite walls. An overview of all the characteristics of the materials can be found in the Supporting Information S1.

2.1.2 | Amines

(3-aminopropyl)trimethoxysilane (APTMS, 97%) and anhydrous diethyl ether (Et_2O, 99%) were obtained from Sigma Aldrich. 3-[2-(2-aminoethylamino)-ethylamino]-propyltrime-thoxysilane (TRI) was purchased from Thermo Fischer Scientific. All chemicals were used as obtained, with no further purification, and stored in an argon atmosphere once opened.

2.2 | Functionalization procedure

The grafting method was based on the dry-gel tumbling procedure described by Kolle and Sayari[25] for silica powder, then scaled and adapted to structured sorbents. The procedure was further optimized for repeatability, which was achieved only when carried out under anhydrous conditions. The same procedure was used for all substrates, alumina loadings, and amine types. The alumina-coated monoliths were dried at 120°C and under vacuum overnight to remove any residual moisture and physisorbed CO_2. Analogously, the stainless-steel reactor used for the functionalization underwent multiple argon-vacuum cycles to remove residual oxygen and moisture before being filled with an argon atmosphere. Then, a solution of 500 mL of Et_2O and a predetermined amount of amines (1:1 ratio - 1 mL amine per g alumina coating) was introduced in the reactor and stirred for 20 min at room temperature to homogenize. In a sensitivity analysis, the ratio of amines to amount of alumina was increased to test if more amines could be immobilized on the surface. However, no advantage was observed, which is why a 1:1 ratio was kept throughout the study. The dried monolith was then suspended from the lid and immersed in the solution by opening the reactor as quickly as possible under an inert atmosphere. The total volume of solution was chosen such that the monolith would be completely submerged inside the reactor. To allow for the amines to be distributed along the entire monolith, the mixture was stirred in an upright position for 2 hours at room temperature. Subsequently, the solvent was removed under low vacuum. The remaining material was subjected to a thermal treatment in a vacuum oven at 110°C for 4.5 hours, followed by cooling overnight. To ensure complete functionalization, a second thermal treatment was performed at 80°C for 4 hours. The setup needed for the functionalization is shown in Figure 2. The functionalization procedure relies on a standard laboratory setup (Schlenk-line) with a custom

15475905, 2026, 10, Downloaded from https://aiche.onlinelibrary.wiley.com/doi/10.1002/aic.70513 by Imperial College London, Wiley Online Library on [15/09/2026]. See the Terms and Conditions (https://onlinelibrary.wiley.com/terms-and-conditions) on Wiley Online Library for rules of use; OA articles are governed by the applicable Creative Commons License

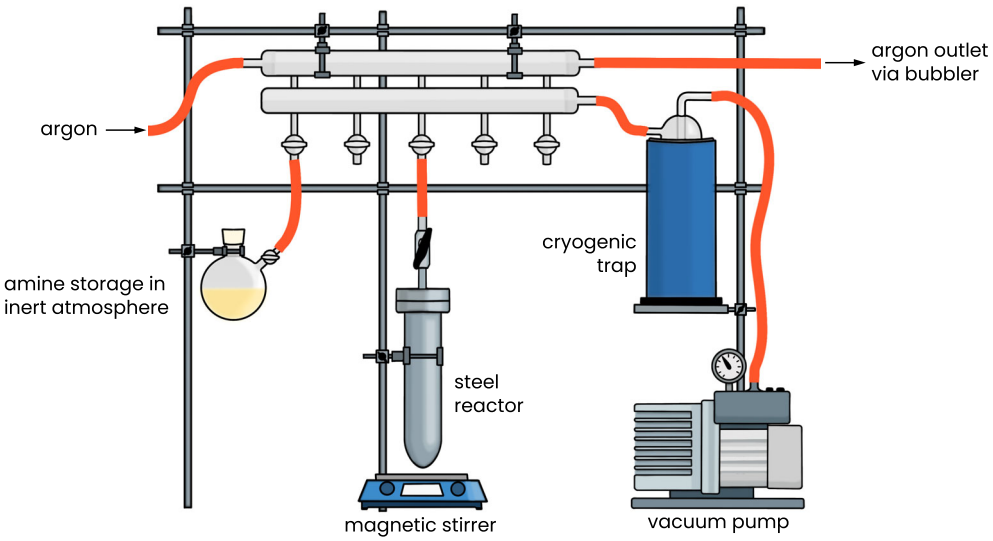


FIGURE 2 Illustration of the experimental setup used to functionalize the monolithic sorbents. The setup includes the amine storage flask, a custom stainless-steel reactor where the monolith is immersed, a magnetic stirrer for homogenization, and a vacuum pump with a cryogenic trap to remove solvents. An argon gas supply maintains an inert atmosphere throughout the process, with an outlet via a bubbler.

stainless-steel reactor adapted to fit the monolithic sample. Note that the same procedure and thermal treatment was applied to both TRI and APTMS. Initial tests showed that neither amine species oxidized at high temperatures, which differs from the findings of Kolle and Sayari.[25] We believe that oxidation could be avoided because the sealed steel reactor could guarantee vacuum during the entire thermal treatment. Overall, the functionalization procedure is robust, simple, and does not require highly specialized equipment beyond an appropriately sized reactor and standard inert-atmosphere handling.

The weight of the monoliths was measured before and after the functionalization procedure to determine the amount of amines, m_{amine}, immobilized on the monolith. The monoliths are always weighed in a dried, regenerated state, that is, after being exposed to vacuum and elevated temperatures, to ensure that only the weight of the material and not adsorbate is recorded. The amine loading, w_{amine}, in the active sorbent is defined as:

$$w_{amine} = \frac{m_{amine}}{m_{al}} \tag{2}$$

The total weight, m, of each sample is the sum of the mass of substrate, alumina, and amines:

$$m = m_{sub} + m_{al} + m_{amine} = m_{sub}(1 + \alpha + \alpha w_{amine}) \tag{3}$$

2.3 | X-ray Computed Tomography scans

The uniformity of the distribution of the immobilized amines along the monoliths can be validated using X-ray Computed Tomography (XCT).[37] The setup used in this work was adapted from Pini et al.[46] The XCT scans were performed using a medical scanner (Toshiba Aquilion 64) in helical mode, applying a peak tube voltage of 120 kV and a current of 200 mA. The quantity measured in the scans is reported as a CT number in Hounsfield Units [HU]. Within a moderate density range, the CT number is linearly proportional to the bulk density of the material.[46]

The output of the XCT scans is a map with a resolution of $512 \times 512 \times 287$ voxels, with a voxel dimension of $0.093\,\text{mm} \times 0.093\,\text{mm} \times 0.5\text{mm}$. For subsequent analysis, the raw image was cropped to a dimension of $306 \times 306 \times 256$ voxels, corresponding to the $3\,\text{cm} \times 3\,\text{cm} \times 13\,\text{cm}$ monolith dimensions. For data analysis, the raw XCT image data were processed to identify the voxels corresponding to the monolith structure from voxels belonging to channel voids. As the air-filled voids have a significantly lower CT number than the solid, the segmentation was performed using a Otsu thresholding filter.[47] The threshold values are reported in the Supporting Information S2. This segmented data were used to quantify the distribution of the material density, which is affected by the alumina coating and functionalization procedure. Since we are not interested in the absolute CT number (and therefore density) but rather the distribution of density along a sample, the data were re-scaled to a local CT number difference. The local CT number difference is a measure of local material density relative to the least dense cross-section of the monolith. Thereby, this rescaling shows variations in material density:

$$\Delta CT(x,y,z) = CT(x,y,z) - \min_z \left(\frac{1}{XY} \sum_{x,y} CT(x,y,z) \right) \tag{4}$$

where $\Delta CT(x,y,z)$ is the local CT number difference for the voxel at position (x,y,z), $CT(x,y,z)$ is the raw CT number at position (x,y,z), and X and Y are the total number of voxels in the x and y directions, respectively.

2.4 | Isotherm characterization

Unary isotherm measurements were performed in a Microtrac Belsorp Max volumetric adsorption measurement device. A pressure change

15475905, 2026, 10, Downloaded from https://aiche.onlinelibrary.wiley.com/doi/10.1002/aic.70513 by Imperial College London, Wiley Online Library on [15/09/2026]. See the Terms and Conditions (https://onlinelibrary.wiley.com/terms-and-conditions) on Wiley Online Library for rules of use; OA articles are governed by the applicable Creative Commons License

of 0.6% in 20 min was defined as the equilibrium criterion for each measurement point.[48] The measurements were performed using a sample of around 1 g of crushed monolith. As the adsorption properties are not homogeneous across the monolith, a sample from the inner channels of a slice in the center of the monolith was chosen for the measurement to avoid edge artifacts. Prior to each measurement, the sorbents were regenerated at 100°C under high vacuum for 3 hours. The CO_2 sorption measurements were performed in a range of 0 to 0.1 bar, and the equilibrium uptake value at 400 ppm was interpolated using the modified Akima method.[49]

2.5 | Breakthrough experiments

The adsorption performance of the monoliths was characterized in both dry and humid DAC conditions using a dynamic column breakthrough setup developed and presented in previous studies.[45,48,50,51] The column was designed to accommodate large samples. In particular, monoliths can be characterized in one piece, without requiring any crushing or partial extraction of the material, which could introduce sampling bias.[14] The contactor consisted of a thermostated jacketed column with a square cross-section of 3.2 cm × 3.2 cm which allowed adding a textile felt between the monolith and column wall to avoid channeling. A conical flange and gas distributor were installed at the column inlet to facilitate homogeneous gas distribution across the full cross-section of the monolith.[45] The inlet flow is humidified using a Controlled Evaporation Mixing (CEM) system (Bronkhorst), in which liquid water from a pressurized reservoir is finely dispersed, mixed with the carrier gas, and subsequently vaporized. This configuration enables accurate control of inlet humidity over a wide dynamic range. To prevent condensation, all gas lines are maintained above the dew point using resistive heating elements.[48] The gas composition at the outlet of the column was determined with a flow-through, non-dispersive infrared CO_2 sensor (Vaisala GMP343) capable of measuring CO_2 concentrations in the range from 0 to 2000 ppm and a flow-through capacitive relative humidity sensor (Rotronic). The inlet can be connected to either pure N_2 (purity 5.0, Linde), or a pre-mixed 400 ppm CO_2 in N_2 (±1% relative purity, Linde) gas bottle.

Prior to each breakthrough run, the sorbents were regenerated at 100°C under a N_2 purge at 0.5 mmol s^{-1} to remove all of the adsorbed water and CO_2. The column was then cooled under a continuous N_2 flow and closed, once the target adsorption temperature of 24°C was reached. To perform the adsorption step of the breakthrough experiment, a bypass line was used to condition a stream of 400 ppm CO_2 in N_2 to the desired relative humidity. Once stable conditions were reached and the variation in the relative humidity signal is below 1%, the stream was redirected through the column ($t = 0$), exposing the sorbent to a humid flow of 0.5 mmol s^{-1} under active cooling. The breakthrough measurements were stopped when the outlet CO_2 concentration reached at least 95% of the feed concentration (t_∞), as the breakthrough curves of the monolith exhibit a long tail, meaning that reaching full saturation would take significantly more time than reaching the first 95%, making it impractical for routine measurements.[48] The breakthrough uptake q_i of species i can then be computed by integrating the mass balance over the column:

$$q_i = \int_0^{t_\infty} \left(N_{\text{in}} y_{\text{in},i} - N_{\text{out}} y_{\text{out},i}(t)\right) \mathrm{d}t \tag{5}$$

where N is the total molar flow, and y_i is the concentration in the gas phase of species i. Note, that we neglect the accumulation of CO_2 in the voids.

The mass flow controllers allow to set and measure the molar flow rate $N_{\text{in,dry}}$ of the dry gas, before it is humidified. The resulting relative humidity is measured downstream during equilibration. From the corresponding water mole fraction, y_{in,H_2O}, the inflowing total molar flow rate, N_{in}, is computed as:

$$N_{\text{in}} = \frac{N_{\text{in,dry}}}{1 - y_{in,H_2O}} \tag{6}$$

Since N_2 is considered inert,[12,14] its molar flow rate at the outlet is assumed to be the same as that at the inlet. A mole balance across the column yields the following expression for the total flow rate at the outlet:

$$N_{\text{out}} = \frac{N_{\text{in,dry}}}{(1 - y_{\text{in},H_2O})} \frac{1 - y_{\text{in},H_2O} - y_{\text{in},CO_2}}{1 - y_{\text{out},H_2O}(t) - y_{\text{out},CO_2}(t)} \tag{7}$$

where y_{in,CO_2} is given by the bottle composition, y_{in,H_2O}, and $N_{\text{in,dry}}$ are controlled, and $y_{\text{out},CO_2}(t)$ and $y_{\text{out},H_2O}(t)$ are measured.

3 | RESULTS

3.1 | Validation of the functionalization procedure

The functionalization of structured sorbents should ensure a homogeneous distribution of the active material, that is, the amines, throughout the structure, a challenge distinct from that of functionalizing powders or pellets. The uniformity of the active sorbent can be validated with XCT scans,[37] as described in Section 2.3. XCT scans were performed for seven mullite samples: one non-functionalized sample, 3 APTMS functionalized samples, and 3 TRI functionalized samples. Figure 3 shows the full three-dimensional processed image obtained from the XCT scans for one exemplary functionalized mullite monolith (M1). An analysis of the front view (center right) and of the cross-sectional cuts (center left) reveals distinct variations in material density: the highest density is observed at the intersections of the channel walls, within the walls of the outer region of the cross-section, and at the edges of the monolith.

To investigate the distribution of density in more detail, we compute the average CT number difference over each cross-section (see Figure 4). A consistent trend can be observed: the average density is higher in the first and the last 20 mm of the monolith and is constant and lower in the central part. In the case of the baseline sample M0

15475905, 2026, 10, Downloaded from https://aiche.onlinelibrary.wiley.com/doi/10.1002/aic.70513 by Imperial College London, Wiley Online Library on [15/09/2026]. See the Terms and Conditions (https://onlinelibrary.wiley.com/terms-and-conditions) on Wiley Online Library for rules of use; OA articles are governed by the applicable Creative Commons License

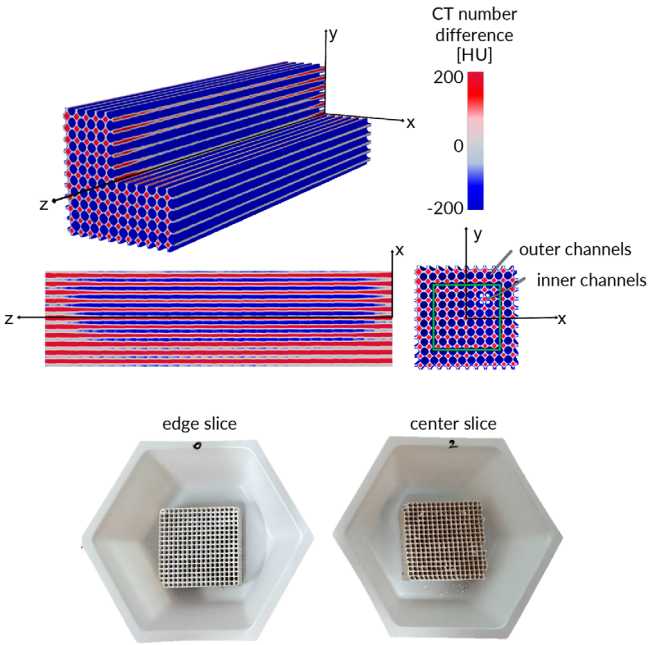


FIGURE 3 Raw results of the XCT scans for an exemplary functionalized mullite monolith (M1). The color bar indicates CT number difference in Hounsfield Units [HU] with respect to the minimal average density of a slice (Equation 4). Top: full 3D view of the monolith with a cutout. Center left: cross-sectional cut through a center wall in the x-z plane. Center right: front view. The green box highlights the segmentation into inner and outer channels. Bottom: Photos of an edge and center slice of a cordierite monolith with high alumina loading showing the visible differences in the distribution of the white alumina coating.

(average CT number $= -265$ HU), the observed density range of $\Delta CT = 40$ HU corresponds to a relative density variation of 7.5%.

When segmenting the data into an inner and outer region of the cross section (see the center right panel in Figure 3 for reference), the outer region consistently exhibits a higher average density than the inner region. For clarity, Figure 4 shows the resulting profiles of the inner and outer regions for M1 only, but all monoliths exhibit similar profiles (see Supporting Information S3). The higher measured density suggests an accumulation of material and, consequently, a potentially higher uptake in the outer regions of the monolith, which is consistent with prior observations reported by Grossmann et al.,[14] who used the same coated monolith support. Note that the local change in density does not equate to a change in open channel cross-section. In the scanned mullite monoliths, the alumina is primarily housed within the internal pore structure of the ceramic matrix rather than accumulating as a thick surface layer.

In order to understand whether this non-uniformity is caused by the functionalization procedure, we can use the XCT scan of the non-functionalized baseline sample (M0) with the same alumina loading (top panel, gray line) as a reference. The scan reveals that the spatial distribution of density is introduced by the alumina coating. This heterogeneity of the alumina is even more pronounced for high alumina loadings. The photos in the bottom panel of Figure 3 show that the edge slice has a visibly thicker white alumina layer, while the center slice exhibits noticeably less alumina, as evidenced by the yellow color of the bare substrate. Both mullite and cordierite monoliths were coated by dipping the monoliths into an alumina-containing dispersion, followed by calcination. During such a dip-coating process, local differences in slurry retention, drainage, capillary forces, and drying can lead to the accumulation of alumina near the outer channels, wall intersections, and monolith ends. The heterogeneity could be reduced by optimizing the wash-coating procedure, for example, by adjusting the slurry viscosity, controlling drying conditions, applying multiple thinner coating steps, or using forced-flow coating rather than simple immersion. However, a systematic optimization of the industrial wash-coating process was outside the scope of the present work.

The analysis of the non-functionalized sample suggests that the main driver for the observed distribution of density is the alumina coating. Still, the TRI functionalized Samples M5 and M6 seem to have a more pronounced heterogeneity in the distribution of density. It is possible that the higher viscosity of TRI results in a maldistribution of amines along the monolith. Since the samples were not scanned before and after functionalization, the accumulation of material in the last 30 mm cannot be clearly attributed to alumina or amines. While

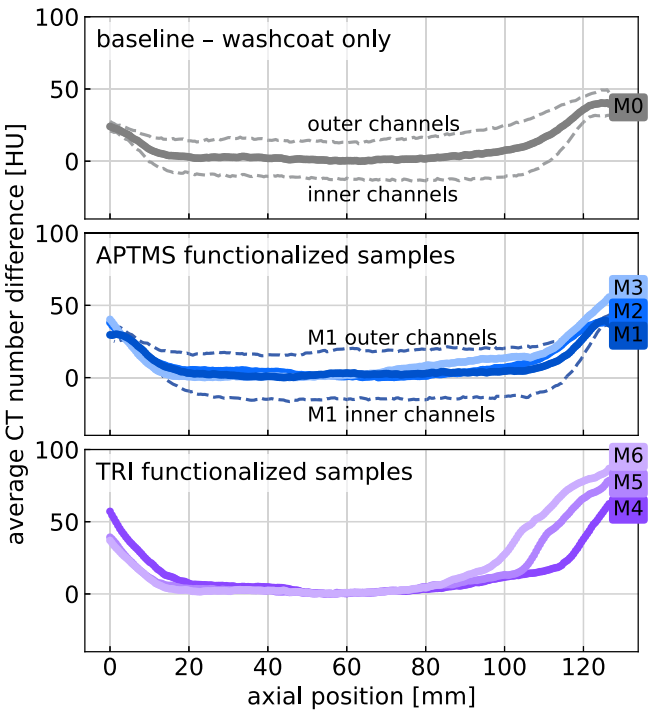


FIGURE 4 Average CT number difference (Equation 4) profiles over the cross-section along the axial position (z-coordinate) for unfunctionalized and functionalized monoliths. The values are rescaled so the minimum average density of each profile is equal to 0. The solid lines denote the average over the entire cross section, while the dashed lines denote the average over the inner and outer region of the cross section. Top (grey): baseline of a alumina coated but unfunctionalized monolith (M0). Center and bottom: monoliths functionalized with APTMS (blue) and TRI (purple), respectively. All samples have an alumina loading of ~ 10 wt.%.

15475905, 2026, 10, Downloaded from https://aiche.onlinelibrary.wiley.com/doi/10.1002/aic.70513 by Imperial College London, Wiley Online Library on [15/09/2026]. See the Terms and Conditions (https://onlinelibrary.wiley.com/terms-and-conditions) on Wiley Online Library for rules of use; OA articles are governed by the applicable Creative Commons License

an independent compositional analysis of solid samples taken from different locations within the monolith could provide complementary confirmation of these spatial variations, such methods are inherently destructive. In this study, non-destructive characterization using XCT were prioritized, to assess the full-sample axial and radial variations without introducing sampling bias.

In conclusion, the XCT scans confirm that the functionalization yields a rather uniform distribution of amines, in particular for APTMS, relative to the existing (heterogeneous) alumina coating. In the future, it would be desirable to calibrate the density variance to a thickness metric to better quantify the distribution of the alumina coating. This would require XCT scans of the exact same monolith samples both before and after the coating process.

The total amount of amines immobilized on each monolith (Figure 5) was quantified using a gravimetric method. Both mullite and cordierite substrates functionalized with APTMS show a clear linear relationship between the mass of alumina and immobilized amines. The data show that the procedure is robust with respect to alumina loading and substrate type, as the functionalization results in a consistent amine loading of $w_{amine} = 0.5$, on average, for all material configurations. A linear regression through all APTMS samples yields an R^2 value of 0.97, indicating that the alumina amount is the dominant factor governing the total quantity of immobilized amines. Note that the independence of the immobilized amount on the substrate type is not obvious, as the substrates have different channel sizes and pore

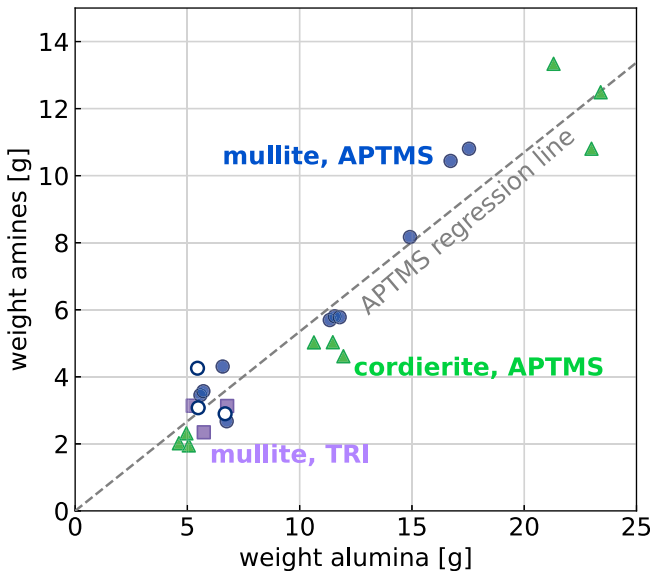


FIGURE 5 Weight of immobilized amines as a function of the weight of the alumina coating for different substrate and amine types: TRI-functionalized mullite monoliths (purple squares), and APTMS-functionalized mullite (blue circles) and cordierite monoliths (green triangles). The sensitivity analysis on the initial amine-to-alumina ratio added in the functionalization procedure (empty circles 1:1.5 ratio and filled blue circles 1:1 ratio) shows overlapping populations, confirming that the 1:1 ratio is sufficient. The dashed line indicates a linear regression for all APTMS samples ($R^2 = 0.97$), highlighting a constant amine loading across varying alumina weights.

distributions, which could potentially affect the effectiveness of the immobilization procedure.

While the overall trends in Figure 5 are clear, the reproducibility of individual samples is not perfect. The regression line indicates that 97% of the variability in the immobilized amine mass can be attributed to changes in alumina loadings. Still, a noticeable scatter remains for samples with similar alumina loadings. The scattering indicates that, for a fixed alumina amount, sample-to-sample variability persists. Several features contribute to this variability: First, ceramic solid supports are inherently non-homogeneous. Second, the XCT scans reveal that spatial variations in alumina distribution are introduced during the alumina coating procedure (see Figures 3 and 4). Third, the functionalization step may introduce additional variability related to amine transport and reaction within the porous alumina layer. In the case of the cordierite samples used in this work, in particular, the small channel which could represent a significant resistance to amine transport, resulting in increased variability compared to the mullite samples. Finally, the gravimetric method itself can contribute to the uncertainty.

Such variability is not uncommon in materials used for DAC.[35,52] The variability emphasizes the critical importance of reporting results from multiple samples rather than relying on a single data point. Consequently, the discussion in the remainder of this work focuses on general trends and averaged behavior.

The functionalization procedure can cause sample-to-sample variability if the procedure fails to fully saturate all available grafting sites on the alumina surface with amines. In the functionalization procedure (see Section 2.2), the dried monoliths are immersed in an anhydrous solution of diethyl ether and amine for two hours before the solvent is removed, and the material undergoes sequential thermal treatments to ensure complete covalent grafting. The initial ratio of alumina to amines added to the solution during the procedure could potentially control the amount of amines immobilized onto the monoliths, thereby introducing variability. To ensure that sufficient amines were added to the solution and that all available grafting sites are saturated, a sensitivity analysis was performed on mullite samples with similar alumina loading using APTMS amines. The baseline protocol uses a 1:1 ratio of alumina to amines in solution, which corresponds to adding 1 mL of amine per g of alumina (represented by the filled blue circles in Figure 5). For the four tested samples, the baseline protocol resulted in an average amine loading of $w_{amine} = 0.57$. The ratio was then varied to 1:1.5 (i.e., 1.5 mL of amine per g of alumina), and three monoliths with the same alumina loading range were functionalized (represented by the empty blue circles in Figure 5). The resulting monoliths had a similar average amine loading of $w_{amine} = 0.59$; Figure 5 clearly shows that the two populations largely overlap. These results suggest that an amine-to-alumina ratio of 1:1 is sufficient, and the amount of amines immobilized on the surface is limited by the (given) amount of alumina coating. Consequently, given the higher amine efficiency (i.e., less amine waste) of the 1:1 ratio, this protocol was adopted for all other amine types, substrate types, and alumina loadings in this study.

In summary, several robust trends emerge from Figures 3 to 5: The XCT analysis demonstrates that the amine distribution closely

15475905, 2026, 10, Downloaded from https://aiche.onlinelibrary.wiley.com/doi/10.1002/aic.70513 by Imperial College London, Wiley Online Library on [15/09/2026]. See the Terms and Conditions (https://onlinelibrary.wiley.com/terms-and-conditions) on Wiley Online Library for rules of use; OA articles are governed by the applicable Creative Commons License

follows the pre-existing alumina distribution, confirming that the grafting procedure results in a uniform distribution of amines relative to the alumina coating. The gravimetric results further show that the grafting procedure is effective for both APTMS and TRI amines, as well as for both mullite and cordierite substrates, and that the amount of immobilized amine scales linearly with the alumina mass. Taken together, these results demonstrate that, while local heterogeneities and sample-to-sample variability are unavoidable, the functionalization procedure is consistent and scalable. This validation provides a solid foundation for the performance analysis presented in the following sections.

3.2 | CO_2 uptake in dry conditions

The validated functionalization procedure allows us to investigate how the CO_2 uptake performance is influenced by the three main material components: substrate, alumina loading, and amine type. The initial investigation focuses on the CO_2 uptake in ultra-dilute (400 ppm), dry conditions at ambient temperature of 25 °C (see Figure 6). The shown amine efficiency is defined as the amount of CO_2 adsorbed per mole of amine group (i.e., mol_{CO_2}/mol_N).

$$\eta_N = \frac{q_{CO_2}}{m_{amine}} \frac{M}{n_N} \tag{8}$$

where q_{CO_2} is the total amount of adsorbed CO_2, m_{amine} is the mass of amines, n_N is the number of amine groups per molecule (i.e., $n_N = 1$ for APTMS and $n_N = 3$ for TRI), and M is the molar mass of the molecule.

At DAC conditions, the measured amine efficiency for the APTMS-functionalized samples is $\eta_N = 0.35$ on average, regardless of the substrate type. In particular, η_N remains constant even with increased alumina weight. In dry conditions, CO_2 adsorption primarily forms ammonium carbamate, which results in a theoretical stoichiometric limit for the amine efficiency of $\eta_N = 0.5$.[15,48,53,54] From Figure 6 (left), we can observe that the TRI-functionalized samples exhibit a significantly lower amine efficiency on average ($\eta_N = 0.2$). Nevertheless, the observed TRI efficiency is comparable to the values measured for TRI-functionalized powders under flue gas conditions,[25] and is even slightly higher than the efficiency of $\eta_N = 0.16$ measured in other TRI-grafted materials under DAC conditions.[14] A possible explanation for the low amine efficiency could be the reduced steric accessibility of the adsorption sites,[16,55] since TRI is a large amine molecule containing one primary and two secondary amines.

The amine efficiency provides insight into the accessibility and utilization of the active sites. However, as a process-relevant KPI, the CO_2 uptake per total mass of sorbent is of primary interest, as it serves as a proxy for the costs and energy consumption of the DAC process[31] (see Figure 6, right). Despite their difference in amine efficiency, TRI and APTMS samples achieve the same total uptake when monoliths of the same support and of similar total weight are compared. Combining the established linear relationship between the mass of amines immobilized and the mass of alumina (Figure 5), with the constant APTMS amine efficiency, leads to a linear relationship between the total CO_2 uptake, alumina weight and therefore total sorbent weight. On average, the CO_2 uptake per unit mass of alumina is $w_{CO_2} = 0.042\ g_{CO_2}/g_{al}$. Importantly, Figure 6 highlights a key difference between the two substrate types: since cordierite has a lower

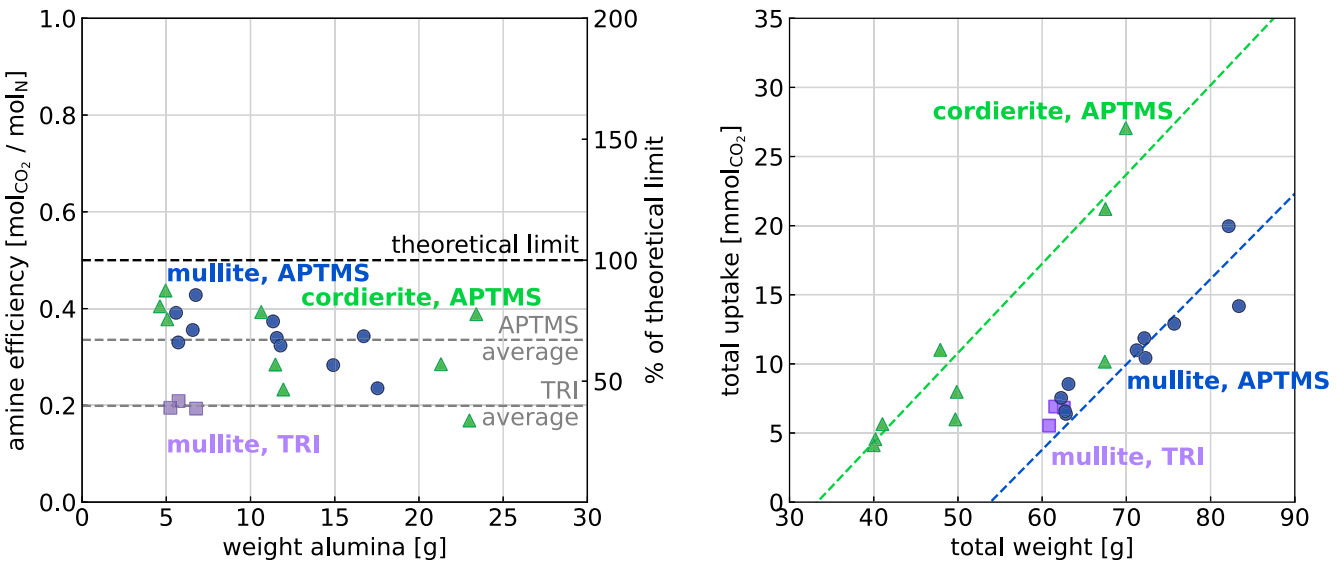


FIGURE 6 CO_2 uptake performance under dry DAC conditions (400 ppm, 25 °C). Left: amine efficiency (Equation 8, mol_{CO_2}/mol_N) as a function of alumina weight, comparing APTMS (blue circles and green triangles) and TRI amines (purple boxes) against the theoretical limit for ammonium carbamate (dotted black line). Right: total CO_2 uptake as a function of total weight of the sample, illustrating the superior process performance achieved by the lighter cordierite substrate (green triangles) compared to mullite (blue circles).

15475905, 2026, 10, Downloaded from https://aiche.onlinelibrary.wiley.com/doi/10.1002/aic.70513 by Imperial College London, Wiley Online Library on [15/09/2026]. See the Terms and Conditions (https://onlinelibrary.wiley.com/terms-and-conditions) on Wiley Online Library for rules of use; OA articles are governed by the applicable Creative Commons License

density (average weight of $m_{sub} = 33$ g per monolith) than mullite (average weight of $m_{sub} = 53$ g per monolith of the same volume), the cordierite samples take up more CO_2 for the same mass of sorbent. For example, a mullite monolith with a total weight of 70 g has an uptake $q_{CO_2} = 10$ mmol, while a cordierite monolith with the same total weight takes up 2.5 times as much CO_2 ($q_{CO_2} = 25$ mmol).

Considering that all tested samples have the same volume, some important process conclusions can be drawn: Increasing the amount of alumina essentially increases the uptake per volume and per total mass because the mass of the inert portion remains constant. Therefore, the total CO_2 yield per energy invested to heat the inert mass increases. This effect is even more pronounced when using low-density ceramics like cordierite. A detailed analysis of the energy demand is provided in Section 3.3. Our results indicate that ideally, the amount of alumina would be increased further, in line with process simulations.[31] However, the maximum alumina loadings used in this study are at the upper limits given by the manufacturers. Hence, the sorbents produced in this work represent the maximum available performance for the given sorbent type.

3.3 | Thermal energy requirements

The energy required for the desorption of CO_2 can be quantified by four components: The sensible heat required to raise the temperature of the substrate from adsorption to desorption conditions, the sensible heats required to raise the temperature of the active sorbent, consisting of alumina and amines, and the latent heat required for desorption, that is, the energy needed to break the amine–CO_2 (and amine–H_2O) chemisorption bonds. Note that analysis neglects water adsorption, as the thermal energy demand for water desorption will qualitatively behave the same as the energy demand for CO_2 desorption. Similarly, we do not include the sensible heat required to heat CO_2 to the desorption conditions, as its contribution is qualitatively equivalent to that of latent heat for CO_2 desorption and is negligible from a quantitative point of view.[56]

The expression for the total energy requirement is therefore:

$$Q = m_{sub} c_{p,sub} \Delta T + m_{al} c_{p,al} \Delta T + m_{amine} c_{p,amine} \Delta T + m_{CO_2} \Delta h_{ads} \quad (9)$$

where m_{sub} is the mass of substrate, m_{al} is the mass of alumina, m_{amine} is the mass of amines, m_{CO_2} is the mass of CO_2 produced per cycle, ΔT is the temperature difference between adsorption and desorption conditions, Δh_{ads} is the absolute value of the isosteric enthalpy of adsorption, and c_p is the specific heat capacity. Note that mullite and cordierite have very similar specific heat capacities but differ in density.[57]

The mass of alumina, m_{al}, can also be expressed in terms of an alumina loading, α, (see Equation (1)) that is, $m_{al} = \alpha m_{sub}$. Equivalently, the mass of amines, m_{amine}, can be expressed as a function of the alumina loading, α, and the amine loading, w_{amine}, (see Equation (2)) that is, $m_{amine} = w_{amine} \alpha m_{sub}$. As reported in Section 3.2, the experimental campaign shows that the CO_2 uptake, and therefore m_{CO_2}, is proportional to the amount of alumina in the sorbent. In particular, the amount of CO_2 that is adsorbed for a given amount of alumina is independent of the substrate type. By defining w_{CO_2} as the CO_2 uptake per unit mass of alumina, the amount of CO_2 produced per cycle is proportional to the mass of substrate, that is, $m_{CO_2} = w_{CO_2} \alpha m_{sub}$. Note that for the scope of this analysis, we assume that all of the adsorbed CO_2 is desorbed during regeneration in order to be able to use the uptake values measured in Section 3.2. Hence, Equation (9) can be re-written as:

$$Q = m_{sub} \left(c_{p,sub} \Delta T + \alpha c_{p,al} \Delta T + w_{amine} \alpha c_{p,amine} \Delta T + w_{CO_2} \alpha \Delta h_{ads} \right) \quad (10)$$

From Equation (10), the specific heat demand per unit mass of CO_2, $\hat{Q}$, can be written as:

$$\hat{Q} = \frac{Q}{m_{CO_2}} = \underbrace{\frac{c_{p,sub} \Delta T}{w_{CO_2} \alpha}}_{\hat{Q}_{sub}} + \underbrace{\frac{c_{p,al} \Delta T}{w_{CO_2}}}_{\hat{Q}_{al}} + \underbrace{\frac{w_{amine} c_{p,amine} \Delta T}{w_{CO_2}}}_{\hat{Q}_{amine}} + \underbrace{\Delta h_{ads}}_{\hat{Q}_{des}} \quad (11)$$

The specific heat demand consists of four contributions (Figure 7). The normalized CO_2 uptake, w_{CO_2} is independent of substrate type and alumina loading and only depends on the adsorption and desorption temperatures. From the experiments, the average

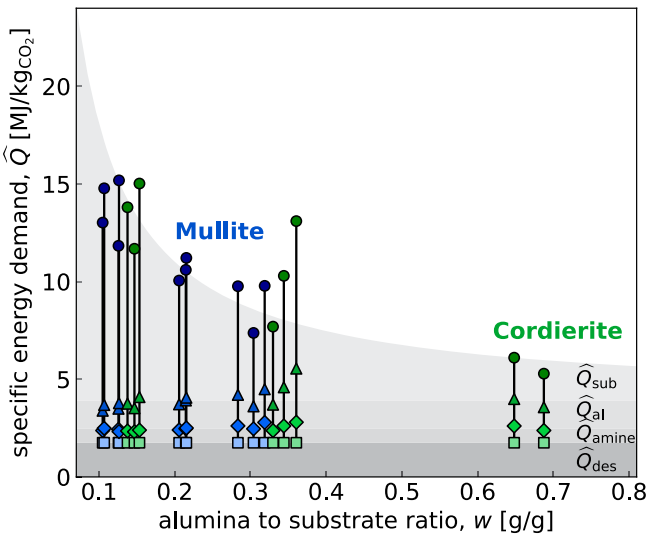


FIGURE 7 Specific thermal energy demand for CO_2 desorption as a function of the alumina to substrate ratio, for $\Delta T = 75$ K and $w_{CO_2} = 0.042\ g_{CO_2}/g_{al}$. A list of all parameter values is provided in the Supporting Information S1. The grey shaded regions illustrate the calculated contributions of the chemical desorption energy ($\hat{Q}_{des}$), and the sensible heat for the amine layer ($\hat{Q}_{amine}$) the alumina coating ($\hat{Q}_{al}$), and the substrate ($\hat{Q}_{sub}$), based on average values (Equation 11). The data points represent values computed from the experimental measurements each sample of adsorbed CO_2 and sample weights (blue: mullite, green: cordierite). The total specific energy demand decreases as alumina loading increases because the CO_2 capture capacity scales linearly with the mass of the alumina, effectively reducing the relative energy cost of heating the inert substrate.

15475905, 2026, 10, Downloaded from https://aiche.onlinelibrary.wiley.com/doi/10.1002/aic.70513 by Imperial College London, Wiley Online Library on [15/09/2026]. See the Terms and Conditions (https://onlinelibrary.wiley.com/terms-and-conditions) on Wiley Online Library for rules of use; OA articles are governed by the applicable Creative Commons License

normalized CO_2 uptake is $w_{CO_2} = 0.042\, g_{CO_2}/g_{al}$. As a result, the heat contributions from the CO_2 desorption, $\hat{Q}_{des}$, heat-up of alumina, $\hat{Q}_{al}$, and heat-up of the amine layer, $\hat{Q}_{amine}$, are independent of the ratio of alumina to substrate mass. The specific energy demand to heat the substrate, $\hat{Q}_{sub}$, however, is inversely proportional to the ratio of alumina to substrate mass, α. Therefore, the specific energy demand can either be reduced by increasing the amount of alumina or by reducing the weight of the substrate.

The analysis of how the alumina loading, α, affects each heat contribution following Equation (11) is based on an ideal, average material. Figure 7 reports the specific energy contributions computed for each sample. In particular, w_{CO_2} depends on the sample. Two observations can be made: (i) in general, the experimental data follow the expected trend: $\hat{Q}_{des}$, $\hat{Q}_{amine}$ and $\hat{Q}_{al}$ are similar for all samples, while $\hat{Q}_{sub}$ decreases with increasing alumina loading. As already observed in Figure 6, the mullite monoliths, where less variation in w_{CO_2} was measured, follow the energy demand trend more closely. (ii) Because cordierite is a lighter substrate, higher ratios of alumina to substrate can be achieved, resulting in a lower demand. The maximum alumina loading achieved by the cordierite samples is 70 wt.%, and 32 wt.% by the mullite samples, respectively (see Figure 7). As the maximum alumina loadings of both substrate types used in this study are at the upper limits given by the manufacturers, this analysis suggests that cordierite is more favorable for DAC applications when optimizing for heat demand.

3.4 | CO_2 uptake in humid conditions

Ambient humidity presents a major challenge for DAC technologies because it can significantly affect the separation efficiency of the sorbent materials and, therefore, process costs.[6–8] Consequently, variations in moisture levels ranging from nearly fully dry climates to highly humid zones must be factored into the material design. The interactions between CO_2, humidity, and the sorbent are highly material-specific. In many cases, these complex interactions trigger opposing effects on both adsorption equilibrium and mass transfer kinetics, making performance difficult to predict across different materials. This complexity is why a thorough characterization of the thermodynamics and kinetics of co-adsorption is required for each material. Here, we therefore compare the performance of the active component of the studied sorbents, that is, the amines, under both dry and humid conditions. To this end, we performed breakthrough experiments under dry DAC conditions (25°C, 400 ppm), as well as representative humid DAC conditions (25°C, 400 ppm, 50% RH) on mullite samples of similar total weight, functionalized with either TRI or APTMS (Figure 8). The reported data are the results of a single breakthrough run. Preliminary repetitions of the humid breakthrough experiments on a subset of samples showed that the observed effect was constant over the repetitions.

Two observations are worth making: From a thermodynamic standpoint, the results show that the CO_2 uptake increases for both

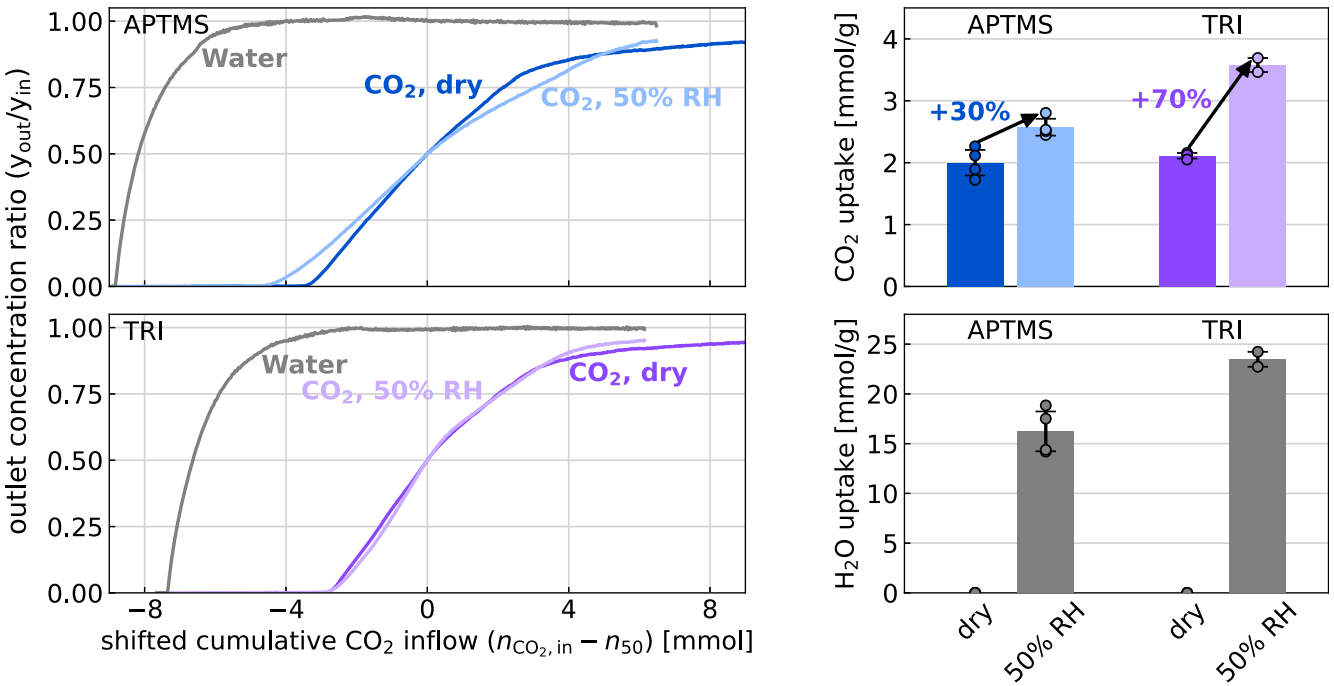


FIGURE 8 Comparison of CO_2 and H_2O co-adsorption thermodynamics and kinetics under dry (400 ppm CO_2, 25°C) and humid (400 ppm CO_2, 25°C, 50% RH) DAC conditions for APTMS (M3) and TRI (M5) amines immobilized on mullite monoliths with an amine loading of ~ 10 wt.%. The gray data corresponds to H_2O adsorption, the blue data to CO_2 adsorption on APTMS, and the purple data to CO_2 adsorption on TRI. Left: Effect of humidity on the steepness of the breakthrough curves. On the x-axis, the cumulative CO_2 inflow, n_{CO_2},in, is shifted by the halfway value, n_{50}. Right: the bar charts quantify the average CO_2 uptake (top) and co-adsorbed H_2O uptake (bottom) per mass of amines, showing a larger enhancement effect for the TRI samples compared to APTMS. The points denote the measured values for each individual sample, and the error bars denote the standard deviation.

15475905, 2026, 10, Downloaded from https://aiche.onlinelibrary.wiley.com/doi/10.1002/aic.70513 by Imperial College London, Wiley Online Library on [15/09/2026]. See the Terms and Conditions (https://onlinelibrary.wiley.com/terms-and-conditions) on Wiley Online Library for rules of use; OA articles are governed by the applicable Creative Commons License

amine types when switching from dry to 50% RH conditions. However, the magnitude of the increase in uptake in the presence of humidity depends distinctly on the amine type: The APTMS-functionalized samples take up 30% more CO_2, while the TRI-functionalized samples show a much larger increase of 70%. The increased uptake measured in this study is in line with observations on TRI samples by Grossmann et al.[48] The observed cooperative effect of water and CO_2 is explained by many different mechanisms in the literature: On the one hand, the increase in uptake is attributed to the formation of new adsorbate species, which possess a higher theoretical amine efficiency compared to the carbamate pathway prevalent in dry conditions,[48,54] which would affect both amine types the same way. On the other hand, the increase in uptake is explained by considering the accessibility of the adsorption site. The co-adsorption of water can cause polymeric structures to swell[58,59] enhancing sorption or catalytically enhance the dry adsorbates.[60] As discussed in the previous section, the TRI-functionalized samples showed a lower amine efficiency compared to APTMS-functionalized samples, suggesting reduced steric accessibility. Thus, the effect of the increase in accessibility is much more pronounced for the TRI samples. The average amine efficiency of the TRI samples increases from $\eta_N = 0.2$ under dry conditions to $\eta_N = 0.32$ under humid conditions.

The second observation is made from the breakthrough curves, which provide information on mass transfer kinetics (Figure 8, left panel). Note that to highlight the breakthrough kinetics, the cumulative CO_2 inflow, n_{CO_2},in, is shifted by the halfway value, n_{50}, such that the curves intersect when the outlet concentration reaches 50% of the inlet concentration. In dry conditions, both APTMS and TRI breakthrough curves exhibit a noticeable long tail. both the APTMS and TRI curve begin to flatten when $n_{CO_2}, \text{in} - n_{50} = 3$ mmol. This long tail indicates resistance to mass transfer within the amine layer.[45,61,62] A key kinetic observation is that the presence of humidity eliminates this long tail, in particular, in the case of APTMS. The change in the shape of the breakthrough curves suggests that water does not only aid the thermodynamics of the process but also facilitates the adsorption kinetics, likely by increasing the driving force and enhancing molecular mobility within the amine layer or promoting faster reaction pathways.

4 | CONCLUSION

This work validates a robust and scalable functionalization procedure to immobilize amines onto alumina by applying the procedure to structured sorbents, consisting of an inert ceramic substrate, a microporous alumina coating, and covalently grafted amines. The functionalization procedure was used to systematically investigate the isolated effect of three independent material components: substrate type, alumina loading, and amine type for DAC applications, thereby providing a versatile platform for material and process design.

X-ray computed tomography and gravimetric analysis demonstrated that the proposed functionalization protocol yields a homogeneous distribution of amines relative to the alumina coating for different substrate types, alumina loadings, and types of amines. In particular, the amount of immobilized amine and CO_2 adsorption capacity were shown to scale linearly with the alumina mass, independent of the substrate morphology. This result indicates that the total amount of the active phase is primarily governed by the amount of alumina support available.

From a process perspective, the comparison between the substrate materials revealed that the lower bulk density of cordierite allows for higher CO_2 uptake per total mass of sorbent compared to mullite. This finding suggests that low-density substrates are highly desirable for reducing the thermal energy required to heat the inert mass of the contactor during the regeneration phase of DAC cycles. As an extension, pure alumina monoliths could be considered as an alternative architecture to reduce the amount of inert material while maximizing the available alumina surface for amine grafting. However, concerns regarding the mechanical and structural stability of pure alumina substrates motivated the design choice in this work to retain a mechanically robust ceramic substrate.

Finally, the characterization of these materials under representative humid DAC conditions highlighted the profound influence of humidity on capture performance: the presence of water was found to enhance process performance regarding both adsorption thermodynamics and kinetics for all investigated materials. In particular, humidity was found to eliminate the characteristic long mass-transfer tails in breakthrough curves for APTMS experiments, suggesting that water facilitates molecular mobility and enables faster reaction pathways within the amine layer. The effects of humidity also depend on the amine type, with TRI-functionalized samples exhibiting a substantially larger increase in CO_2 uptake in the presence of humidity compared to APTMS-functionalized samples, underlining the importance of characterizing sorbents in realistic operating environments.

Overall, this study establishes clear material performance relationships for amine-grafted monolithic sorbents under direct air capture conditions. The presented data set provides a quantitative foundation for cycle modeling, process design, and contactor optimization. More broadly, the results demonstrate that structured sorbents with high alumina loadings on lightweight substrates represent a promising material configuration within current manufacturing constraints, thereby offering a realistic pathway toward efficient and scalable DAC contactors.

NOMENCLATURE

α	alumina loading (mass fraction of alumina to substrate) -
ΔCT	CT number difference HU
Δh_{ads}	absolute value of the isosteric enthalpy of adsorption J g^{-1}
η_N	amine efficiency -
ΔT	temperature difference between adsorption and desorption K
$\hat{Q}$	specific heat demand per unit mass of CO_2 J g^{-1}
$\hat{Q}_{al}$	specific sensible heat of alumina J g^{-1}
$\hat{Q}_{amine}$	specific sensible heat of the amine layer J g^{-1}
$\hat{Q}_{des}$	specific latent heat required for CO_2desorption J g^{-1}

15475905, 2026, 10, Downloaded from https://aiche.onlinelibrary.wiley.com/doi/10.1002/aic.70513 by Imperial College London, Wiley Online Library on [15/09/2026]. See the Terms and Conditions (https://onlinelibrary.wiley.com/terms-and-conditions) on Wiley Online Library for rules of use; OA articles are governed by the applicable Creative Commons License

$\hat{Q}_{sub}$	specific sensible heat of the substrate J g^{-1}
c_p	specific heat capacity J g^{-1} K^{-1}
M	molar mass g mol^{-1}
m	total mass of sorbent sample g
m_{al}	mass of alumina g
m_{amine}	mass of amines g
m_{sub}	mass of ceramic substrate g
m_{CO_2}	amount of CO_2produced per cycle g
N	molar flowrate mol s^{-1}
n_N	number of amine groups per moluecule -
Q	total heat demand J
q	total adsorbed amount mol
t_∞	duration of breaktrough experiments s
w_{amine}	amine loading on alumina coating -
w_{CO_2}	CO_2uptake per unit alumina g g^{-1}
y	molar concentration -

AUTHOR CONTRIBUTIONS

Nicole Ferru: conceptualization; investigation; writing – original draft; methodology; validation; visualization; software; formal analysis; data curation. **Moritz Bischof:** investigation; writing – review and editing; formal analysis. **Martina Saporito:** investigation; writing – review and editing; formal analysis. **David Büchner:** investigation; writing – review and editing; formal analysis; methodology. **Quirin Grossmann:** conceptualization; writing – review and editing; methodology. **Vincent Dufour-Décieux:** writing – review and editing; supervision. **Ronny Pini:** writing – review and editing; supervision; resources; methodology. **André Bardow:** conceptualization; writing – review and editing; resources; supervision; funding acquisition. **Marco Mazzotti:** conceptualization; funding acquisition; writing – review and editing; supervision; resources.

ACKNOWLEDGMENTS

The authors thank HUG Engineering and Corning for providing the many wash-coated monoliths. N.F. acknowledges the ETH Foundation for funding her PhD grant for Direct Air Capture research. D. B. gratefully acknowledges the financial support provided through a PhD scholarship from the Department of Chemical Engineering, Imperial College London. Open access publishing facilitated by Eidgenossische Technische Hochschule Zurich, as part of the Wiley - Eidgenossische Technische Hochschule Zurich agreement via the Consortium Of Swiss Academic Libraries.

FUNDING INFORMATION

This work was supported by ETH Zürich Foundation and Imperial College London.

DATA AVAILABILITY STATEMENT

The numerical data from Figures 5–7 are tabulated in the Supporting Information S2. The properties used for the energy calculations in Figure 7 are reported in the Supporting Information S3. The left panel in Figure 8 contains the raw data as obtained from the experimental setup for two samples. The raw data for the other samples is reported in the Supporting Information S4.

Experimental data shown without error bars are from individual experimental measurements. Error bars in Figure 8 indicate one standard deviation in the data. The raw CT scan measurements analyzed in Figure 4, as well as any other data that support the findings of this study are available from the corresponding author upon request.

ORCID

Nicole Ferru https://orcid.org/0009-0000-6466-5149
Moritz Bischof https://orcid.org/0009-0005-3057-0041
Martina Saporito https://orcid.org/0009-0000-8604-9558
David Büchner https://orcid.org/0009-0004-3813-3455
Quirin Grossmann https://orcid.org/0000-0003-0999-0891
Vincent Dufour-Décieux https://orcid.org/0000-0001-9654-4923
Ronny Pini https://orcid.org/0000-0002-9443-3573
André Bardow https://orcid.org/0000-0002-3831-0691
Marco Mazzotti https://orcid.org/0000-0002-4948-6705

REFERENCES

1. UNFCCC. The Paris agreement. 2018 https://unfccc.int/process-and-meetings/the-paris-agreement
2. IPCC. *Global Warming of 1.5°C: IPCC Special Report on Impacts of Global Warming of 1.5°C above Pre-Industrial Levels in Context of Strengthening Response to Climate Change, Sustainable Development, and Efforts to Eradicate Poverty*. 1st ed. Cambridge University Press; 2022.
3. Bui M, Adjiman CS, Bardow A, et al. Carbon capture and storage (CCS): the way forward. *Energ Environ Sci*. 2018;11:1062-1176.
4. Van Der Spek M. An ecosystem of carbon dioxide removal reviews – part 1: direct air CO_2 capture and storage. *Energ Environ Sci*. 2025;18:9713-9785.
5. Realmonte G, Drouet L, Gambhir A, et al. An inter-model assessment of the role of direct air capture in deep mitigation pathways. *Nat Commun*. 2019;10:3277.
6. Terlouw T, Pokras D, Becattini V, Mazzotti M. Assessment of potential and techno-economic performance of solid sorbent direct air capture with CO_2 storage in Europe. *Environ Sci Technol*. 2024;58:10567-10581.
7. Wiegner JF, Grimm A, Weimann L, Gazzani M. Optimal design and operation of solid sorbent direct air capture processes at varying ambient conditions. *Ind Eng Chem Res*. 2022;61:12649-12667.
8. Sendi M, Bui M, Dowell NM, Fennell P. Geospatial analysis of regional climate impacts to accelerate cost-efficient direct air capture deployment. *One Earth*. 2022;5:1153-1164.
9. Young J, García-Díez E, Garcia S, Van Der Spek M. The impact of binary water–CO_2 isotherm models on the optimal performance of sorbent-based direct air capture processes. *Energ Environ Sci*. 2021;14:5377-5394.
10. Didas SA, Kulkarni AR, Sholl DS, Jones CW. Role of amine structure on carbon dioxide adsorption from Ultradilute gas streams such as ambient air. *ChemSusChem*. 2012;5:2058-2064.
11. Kumar A, Madden DG, Lusi M, et al. Direct air capture of CO_2 by Physisorbent materials. *Angew Chem Int ed Engl*. 2015;54:14372-14377.
12. Low M-YA, Barton LV, Pini R, Petit C. Analytical review of the current state of knowledge of adsorption materials and processes for direct air capture. *Chem Eng Res des*. 2023;189:745-767.
13. Sanz-Pérez ES, Murdock CR, Didas SA, Jones CW. Direct capture of CO_2 from ambient air. *Chem Rev*. 2016;116:11840-11876.

15475905, 2026, 10, Downloaded from https://aiche.onlinelibrary.wiley.com/doi/10.1002/aic.70513 by Imperial College London, Wiley Online Library on [15/09/2026]. See the Terms and Conditions (https://onlinelibrary.wiley.com/terms-and-conditions) on Wiley Online Library for rules of use; OA articles are governed by the applicable Creative Commons License

14. Grossmann Q, Stampi-Bombelli V, Yakimov A, Docherty S, Copéret C, Mazzotti M. Developing versatile contactors for direct air capture of CO_2 through amine grafting onto alumina pellets and alumina wash-coated monoliths. *Ind Eng Chem Res*. 2023;62:13594-13611.
15. Kolle JM, Fayaz M, Sayari A. Understanding the effect of water on CO_2 adsorption. *Chem Rev*. 2021;121:7280-7345.
16. Hack J, Maeda N, Meier DM. Review on CO_2 capture using amine-functionalized materials. *ACS Omega*. 2022;7:39520-39530.
17. Wagner A, Steen B, Johansson G, Zanghellini E, Jacobsson P, Johansson P. Carbon dioxide capture from ambient air using amine-grafted mesoporous adsorbents. *Int J Spectrosc*. 2013;2013:690186.
18. Belmabkhout Y, Serna-Guerrero R, Sayari A. Adsorption of CO_2-containing gas mixtures over amine-bearing pore-expanded MCM-41 silica: application for gas purification. *Ind Eng Chem Res*. 2010;49:359-365.
19. Wurzbacher JA, Gebald C, Steinfeld A. Separation of CO_2 from air by temperature-vacuum swing adsorption using diamine-functionalized silica gel. *Energ Environ Sci*. 2011;4:3584-3592.
20. Choi S, Gray ML, Jones CW. Amine-tethered solid adsorbents coupling high adsorption capacity and Regenerability for CO_2 capture from ambient air. *ChemSusChem*. 2011;4:628-635.
21. Chaikittisilp W, Khunsupat R, Chen TT, Jones CW. Poly(allylamine)–mesoporous silica composite materials for CO_2 capture from simulated flue gas or ambient air. *Ind Eng Chem Res*. 2011;50:14203-14210.
22. Brilman DWF, Veneman R. Capturing atmospheric CO_2 using supported amine sorbents. *Energy Procedia*. 2013;37:6070-6078.
23. Goeppert A, Czaun M, May RB, Prakash GKS, Olah GA, Narayanan SR. Carbon dioxide capture from the air using a polyamine based regenerable solid adsorbent. *J Am Chem Soc*. 2011;133:20164-20167.
24. Wadi B, Golmakani A, Manovic V, Nabavi SA. Evaluation of moderately grafted primary, diamine, and triamine sorbents for CO_2 adsorption from ambient air: balancing kinetics and capacity under humid conditions. *Ind Eng Chem Res*. 2021;60:13309-13317.
25. Kolle JM, Sayari A. Dry gel grafting of mesoporous silica: application to amine-based CO_2 adsorbents. *Microporous Mesoporous Mater*. 2022;343:112195.
26. Kolle JM, Johnson-Omodu N, Sayari A. Environmentally friendly gas phase grafting of mesoporous silicas. *Chem Eng J*. 2022;430:132627.
27. Harlick PJE, Sayari A. Applications of pore-expanded mesoporous silica. 5. Triamine grafted material with exceptional CO_2 dynamic and equilibrium adsorption performance. *Ind Eng Chem Res*. 2007;46:446-458.
28. Elfving J, Bajamundi C, Kauppinen J. Characterization and performance of direct air capture sorbent. *Energy Procedia*. 2017;114:6087-6101.
29. Kaur C, Sayari A. CO_2 uptake – relative humidity – pore size relationship: a new tool for the Design of Amine-Containing Adsorbents. *Chem Eng J*. 2025;512:162716.
30. Rezaei F, Webley P. Optimum structured adsorbents for gas separation processes. *Chem Eng Sci*. 2009;64:5182-5191.
31. Stampi-Bombelli V, Mazzotti M. Exploring geometric properties and cycle Design in Packed bed and Monolith Contactors Using Temperature-Vacuum Swing Adsorption Modeling for direct air capture. *Ind Eng Chem Res*. 2024;63:19728-19743.
32. Gebald C, Piatkowski N, Rüesch T, Wurzbacher JA. Low-pressure drop structure of particle adsorbent bed for adsorption gas separation process. 2014.
33. Eisenberger P. Carbon dioxide capture/regeneration structures and techniques. 2012.
34. Born MH, Denayer JF, Van Assche TR. High capacity laminate Adsorbers: enhancing separation performance beyond packed beds. *Chem Eng J*. 2024;488:150627.
35. Sakwa-Novak MA, Yoo C-J, Tan S, Rashidi F, Jones CW. Poly(ethylenimine)-functionalized monolithic alumina honeycomb adsorbents for CO_2 capture from air. *ChemSusChem*. 2016;9:1859-1868.
36. Darunte LA, Terada Y, Murdock CR, Walton KS, Sholl DS, Jones CW. Monolith-supported amine-functionalized Mg2(dobpdc) adsorbents for CO_2 capture. *ACS Appl Mater Interfaces*. 2017;9:17042-17050.
37. Tegeler E, Cui Y, Masoudi M, et al. A novel contactor for reducing the cost of direct air capture of CO_2. *Chem Eng Sci*. 2023;281:119107.
38. Akhtar F, Kaiser A. Design and structuring of porous sorbents for CO_2 capture and separation. *Curr Opin Green Sustain Chem*. 2024;50:100966.
39. Kim S-Y, Holmes HE, Wang Y, Weston SC, Lively RP. Polymer-sorbent direct air capture contactors with complex geometries 3D-printed via templated phase inversion. *Adv Funct Mater*. 2025;35:2410356. doi:ht10.1002/adfm.202410356
40. Narayanan P, Kim S-Y, Alhazmi D, Jones CW, Lively RP. Self-supported branched poly(ethylenimine) monoliths from inverse template 3D printing for direct air capture. *ACS Appl Mater Interfaces*. 2025;17:10696-10709.
41. Shao Q, Gan Z, Ge B, et al. 3D printing of poly(ethyleneimine)-functionalized Mg-Al mixed metal oxide monoliths for direct air capture of CO_2. *J Energy Chem*. 2024;96:491-500.
42. Wang Y, Rim G, Song M, Holmes HE, Jones CW, Lively RP. Cold temperature direct air CO_2 capture with amine-loaded metal–organic framework monoliths. *ACS Appl Mater Interfaces*. 2024;16:1404-1415.
43. Ryu U, Min YJ, Zhao W, Lee Y, Realff MJ, Jones CW. Climatic conditions and amine loading impact the performance of laminate-supported poly(ethylenimine) direct air capture sorbents. *JACS Au*. 2025;5:6298-6314.
44. Hosseini S, Moghaddas H, Masoudi Soltani S, Kheawhom S. Technological applications of honeycomb monoliths in environmental processes: a review. *Process Saf Environ Prot*. 2020;133:286-300.
45. Stampi-Bombelli V, Storione A, Grossmann Q, Mazzotti M. On comparing packed beds and monoliths for CO_2 capture from air through experiments, theory, and modeling. *Ind Eng Chem Res*. 2024;63:11637-11653.
46. Pini R, Joss L, Hosseinzadeh Hejazi SA. Quantitative imaging of gas adsorption equilibrium and dynamics by X-ray computed tomography. *Adsorption*. 2021;27:801-818.
47. Otsu N. A threshold selection method from Gray-level histograms. *Automatica J IFAC*. 1979;11:285-296.
48. Grossmann Q, Saenz-Cavazos PA, Ferru N, Williams DR, Mazzotti M. Measuring and modeling water and carbon dioxide adsorption on amine functionalized alumina under direct air capture conditions. *Ind Eng Chem Res*. 2025;64:7165-7175.
49. Akima H. A new method of interpolation and smooth curve fitting based on local procedures. *J ACM*. 1970;17:589-602.
50. Joss L, Mazzotti M. Modeling the extra-column volume in a small column setup for bulk gas adsorption. *Adsorption*. 2012;18:381-393.
51. Hefti M, Joss L, Marx D, Mazzotti M. An experimental and modeling study of the adsorption equilibrium and dynamics of water vapor on activated carbon. *Ind Eng Chem Res*. 2015;54:12165-12176.
52. Galanti M, Teunissen R, Roghair I, van Sint Annaland M. Toward consistent thermodynamic modeling of CO_2 adsorption on Lewatit VPOC 1065 under dry conditions: isotherm variability, data gaps, and model fitting. *Curr Opin Chem Eng*. 2026;51:101201.

15475905, 2026, 10, Downloaded from https://aiche.onlinelibrary.wiley.com/doi/10.1002/aic.70513 by Imperial College London, Wiley Online Library on [15/09/2026]. See the Terms and Conditions (https://onlinelibrary.wiley.com/terms-and-conditions) on Wiley Online Library for rules of use; OA articles are governed by the applicable Creative Commons License

53. Hamdy LB, Goel C, Rudd JA, Barron AR, Andreoli E. The application of amine-based materials for carbon capture and utilisation: an overarching view. *Mater Adv*. 2021;2:5843-5880.
54. Yu J, Chuang SSC. The role of water in CO_2 capture by amine. *Ind Eng Chem Res*. 2017;56:6337-6347.
55. Al Araj H, Bahamon D, Reddy KSK, Vega LF, Karanikolos GN. A systematic approach to understanding and optimizing the CO_2 capture performance of triamine-functionalized mesoporous silica with amine blends using molecular simulations. *J Phys Chem C*. 2023;127:7410-7424.
56. Antunes Morgado N, Ferru N, Bardow A, Mazzotti M. Direct air capture by direct steam heating - experiments and comparison with indirect heating. *Chem Eng J*. 2026;527:171584.
57. NIST Office of Data and Informatics. NIST chemistry webbook. https://webbook.nist.gov/chemistry/
58. Liu F, Kuang Y, Wang S, Chen S, Fu W. Preparation and characterization of molecularly imprinted solid amine adsorbent for CO_2 adsorption. *New J Chem*. 2018;42:10016-10023.
59. Song A-Y, Young J, Wang J, et al. Discerning molecular-level CO_2 adsorption behavior in amine-modified sorbents within a controlled CO_2/H_2O environment towards direct air capture. *J Mater Chem A*. 2024;12:25875-25886.
60. Said RB, Kolle JM, Essalah K, Tangour B, Sayari A. A unified approach to CO_2–amine reaction mechanisms. *ACS Omega*. 2020;5:26125-26133.
61. Grossmann Q, Mazzotti M. Mass transfer of CO_2 in amine-functionalized structured contactors in ultra-dilute conditions. *Ind Eng Chem Res*. 2025;64:2339-2353.
62. Kalyanaraman J, Fan Y, Lively RP, et al. Modeling and experimental validation of carbon dioxide sorption on hollow fibers loaded with silica-supported poly(ethylenimine). *Chem Eng J*. 2015;259:737-751.

SUPPORTING INFORMATION

Additional supporting information can be found online in the Supporting Information section at the end of this article.

How to cite this article: Ferru N, Bischof M, Saporito M, et al. Structured sorbents for Direct Air Capture: The impact of materials and chemicals on performance. *AIChE J*. 2026; 72(10):e70513. doi:10.1002/aic.70513

15475905, 2026, 10, Downloaded from https://aiche.onlinelibrary.wiley.com/doi/10.1002/aic.70513 by Imperial College London, Wiley Online Library on [15/09/2026]. See the Terms and Conditions (https://onlinelibrary.wiley.com/terms-and-conditions) on Wiley Online Library for rules of use; OA articles are governed by the applicable Creative Commons License